inactivation would arise from a race between the dissociation of a blocker molecule and the dissociation of this K^+ ion (Fig. 3E) (*15*). In support of the idea that the control site is in the pore, we found a substantial voltage dependence for external K^+ binding to the blocked channel, with lower occupancy and thus faster inactivation at more positive voltages (electrical distance of 0.5 ± 0.1) (*16*).

Intracellular open channel blockers can produce use-dependent blockade of K^+ channels by promoting cumulative inactivation in two ways. First, blockade of outward K^+ flux leads to faster inactivation. This effect is sensitive to blocker dwell time and is opposed by external [K^+] in the physiologic range. Second, blockers can exert an allosteric effect on inactivation. Understanding the factors controlling the use dependence of K^+ channel blockers should help the development of better therapeutic agents, particularly in cases in which insufficient or even reverse use dependence is a serious problem for the therapeutic value and safety of channel blockers (*17*).

REFERENCES AND NOTES

1. R. L. Macdonald, *Epilepsia* **30**, S19 (1989); J. T. Bigger and B. F. Hoffman, in *The Pharmacological Basis of Therapeutics*, A. G. Gilman, L. S. Goodman, R. W. Rall, F. Murad, Eds. (Macmillan, New York, 1985), chap. 31.
2. The two accepted models for use-dependent blockade either use an increased affinity of the binding site in the open or inactivated state (the "modulated receptor" model) or trap the blocker in the channel by a closed gate (the "guarded receptor" model) [B. Hille, *J. Gen. Physiol.* **69**, 497 (1977); C. F. Starmer, A. O. Grant, H. C. Strauss, *Biophys. J.* **46**, 15 (1984); J. F. Butterworth and G. R. Strichartz, *Anesthesiology* **72**, 711 (1990)].
3. N-type inactivation occurs by a ball-and-chain mechanism in which the NH_2-terminal portion of the protein acts as a tethered blocker to inactivate the channel [T. Hoshi, W. N. Zagotta, R. W. Aldrich, *Science* **250**, 533 (1990); S. D. Demo and G. Yellen, *Neuron* **7**, 743 (1991)].
4. K. L. Choi, R. W. Aldrich, G. Yellen, *Proc. Natl. Acad. Sci. U.S.A.* **88**, 5092 (1991).
5. T. Hoshi, W. N. Zagotta, R. W. Aldrich, *Neuron* **7**, 547 (1991); G. Yellen, D. Sodickson, T.-Y. Chen, M. E. Jurman, *Biophys. J.* **66**, 1068 (1994).
6. C. M. Armstrong, *J. Gen. Physiol.* **54**, 553 (1969).
7. Abbreviations for the blockers are TEA, tetraethylammonium; C_n-TEA, alkyl (C_nH_{2n+1}) triethylammonium; Br, bretylium; and QX, QX-314 (a quaternary lidocaine derivative with a triethylamino moiety).
8. K. L. Choi, C. Mossman, J. Aubé, G. Yellen, *Neuron* **10**, 533 (1993).
9. T. Baukrowitz and G. Yellen, *ibid.* **15**, 951 (1995).
10. There is a noticeable dependence of inactivation rate on external K^+ under normal conditions of K^+ efflux, but this is much smaller than the effect noted here. It is more pronounced in mutants of the Shaker channel or in other K^+ channels [J. López-Barneo, T. Hoshi, S. H. Heinemann, R. W. Aldrich, *Recept. Channels* **1**, 61 (1993); L. A. Pardo *et al.*, *Proc. Natl. Acad. Sci. U.S.A.* **89**, 2466 (1992); P. Labarca and R. MacKinnon, *Biophys. J.* **61**, A378 (abstr.) (1992)]. Also, the effect of external K^+ in preventing blocker-promoted inactivation was not caused by knock-off of the blockers [as seen, for example, in C. M. Armstrong, *J. Gen. Physiol.* **58**, 413 (1971), and G. Yellen, *ibid.* **84**, 187 (1984)]. This could be ruled out because the degree of blockade did not change with the low concentrations of external K^+, and because there was no difference in the apparent affinity for K^+ measured in either the presence or the absence of blocker (so long as there was no outward flux).
11. B. Hille, *Ionic Channels of Excitable Membranes* (Sinauer, Sunderland, MA, ed. 2, 1992), chap. 11; J. Crank, *The Mathematics of Diffusion* (Clarendon Press, Oxford, UK, ed. 2, 1975).
12. Although most of the experiments presented here were done with external *N*-methylglucamine (NMG), the presence of external Na^+ made no detectable difference (*9*; T. Baukrowitz and G. Yellen, unpublished data).
13. A. L. Hodgkin and R. D. Keynes, *J. Physiol. (London)* **128**, 61 (1955); B. Hille and W. Schwarz, *J. Gen. Physiol.* **72**, 409 (1978).
14. W. Almers and E. W. McCleskey, *J. Physiol. (London)* **353**, 585 (1984); P. Hess and R. W. Tsien, *Nature* **309**, 453 (1984).
15. If more than two K^+ ions are involved in permeation, we cannot be certain that the dwell time we measure is that of the very last K^+ ion remaining: It could be that of the penultimate ion, for example, but not that of the first ion to leave (which must proceed at the rate of permeation).
16. T. Baukrowitz and G. Yellen, data not shown.
17. L. M. Hondeghem and D. J. Snyders, *Circulation* **81**, 686 (1990); but see T. J. Colatsky, C. H. Follmer, C. F. Starmer, *ibid.* **82**, 2235 (1990).
18. Transfection and electrophysiology methods were as previously described (*9*). The basic internal solution was 160 mM KCl, 1 mM EGTA, 0.5 mM $MgCl_2$, and 10 mM Hepes (pH 7.4); in the zero internal [K^+] experiments, K^+ was replaced with NMG. The external solution for Fig. 1, A and D, contained 150 mM NaCl, 3 mM $CaCl_2$, 1 mM $MgCl_2$, and 10 mM Hepes (pH 7.4), and KCl was added at the indicated concentration. All of the other experiments used 160 mM NMG, 3 mM $CaCl_2$, 1 mM $MgCl_2$, and 10 mM Hepes (pH 7.4), in which KCl was substituted for NMG as indicated.
19. Copper (II):phenanthroline (750 μM:3 mM) was applied to the intracellular face of the patch for <1 min to eliminate N-type inactivation [J. P. Ruppersberg *et al.*, *Nature* **352**, 711 (1991)].
20. Power spectra from long pulses were computed by fast Fourier transform (Matlab; Mathsoft, Natick, MA) and fitted to a sum of Lorentzian and 1/*f* noise, where *f* is the frequency. The corner frequency and fractional block were used to compute the off-rate of the blocker.

21. We thank M. Jurman for providing transfected cells and C. Miller for his trenchant advice on the manuscript. Supported by National Institute of Neurological Diseases and Stroke grant NS29693 (G.Y.) and by a stipend from the Gottlieb Daimler–Karl Benz Foundation (T.B.).

15 August 1995; accepted 8 November 1995

Horizontal Cells of the Primate Retina: Cone Specificity Without Spectral Opponency

Dennis M. Dacey,* Barry B. Lee, Donna K. Stafford, Joel Pokorny, Vivianne C. Smith

The chromatic dimensions of human color vision have a neural basis in the retina. Ganglion cells, the output neurons of the retina, exhibit spectral opponency; they are excited by some wavelengths and inhibited by others. The hypothesis that the opponent circuitry emerges from selective connections between horizontal cell interneurons and cone photoreceptors sensitive to long, middle, and short wavelengths (L-, M-, and S-cones) was tested by physiologically and anatomically characterizing cone connections of horizontal cell mosaics in macaque monkeys. H1 horizontal cells received input only from L- and M-cones, whereas H2 horizontal cells received a strong input from S-cones and a weaker input from L- and M-cones. All cone inputs were the same sign, and both horizontal cell types lacked opponency. Despite cone type selectivity, the horizontal cell cannot be the locus of an opponent transformation in primates, including humans.

The retina is the site of two fundamental stages in the neural representation of color. First, the visual image is discretely sampled by three types of cone photoreceptor with different spectral sensitivities (*1*). Only 7 to 10% of the cones are S-cones (*2*); the remainder are L- and M-cones. Second, cone signals interact antagonistically to form spectrally opponent pathways (*3*). In a red-green pathway, signals from L- and M-cones are differenced, and in a blue-yellow pathway, signals from S-cones oppose a combined signal from L- and M-cones. For nearly 40 years, it has been known that these opponent signals are a property of retinal ganglion cells, the output neurons of the retina, yet the interneuronal circuitry that creates the opponent transformation has remained virtually unstudied because of the technical difficulties of making intracellular recordings from the intact retina of primates (*4*, *5*).

In nonmammals with trichromatic vision, horizontal cells—one class of interneuron—display spectral opponency (*6*). A long-held view is that an opponent transformation occurs by cone type–selective negative feedback from horizontal cells to cones (*7*). Indirect evidence for such opponent feedback in primates is conflicting. Boycott and Wässle reported that two horizontal cell types (H1 and H2) contact all cone types nonselectively and should not, therefore, subserve opponency (*8*); the first

D. M. Dacey and D. K. Stafford, Department of Biological Structure, Box 357420, University of Washington, Seattle, WA 98195–7420, USA.
B. B. Lee, Max Planck Institute for Biophysical Chemistry, 37077 Göttingen, Germany.
J. Pokorny and V. C. Smith, Visual Sciences Center, University of Chicago, Chicago, IL 60637, USA.

*To whom correspondence should be addressed.

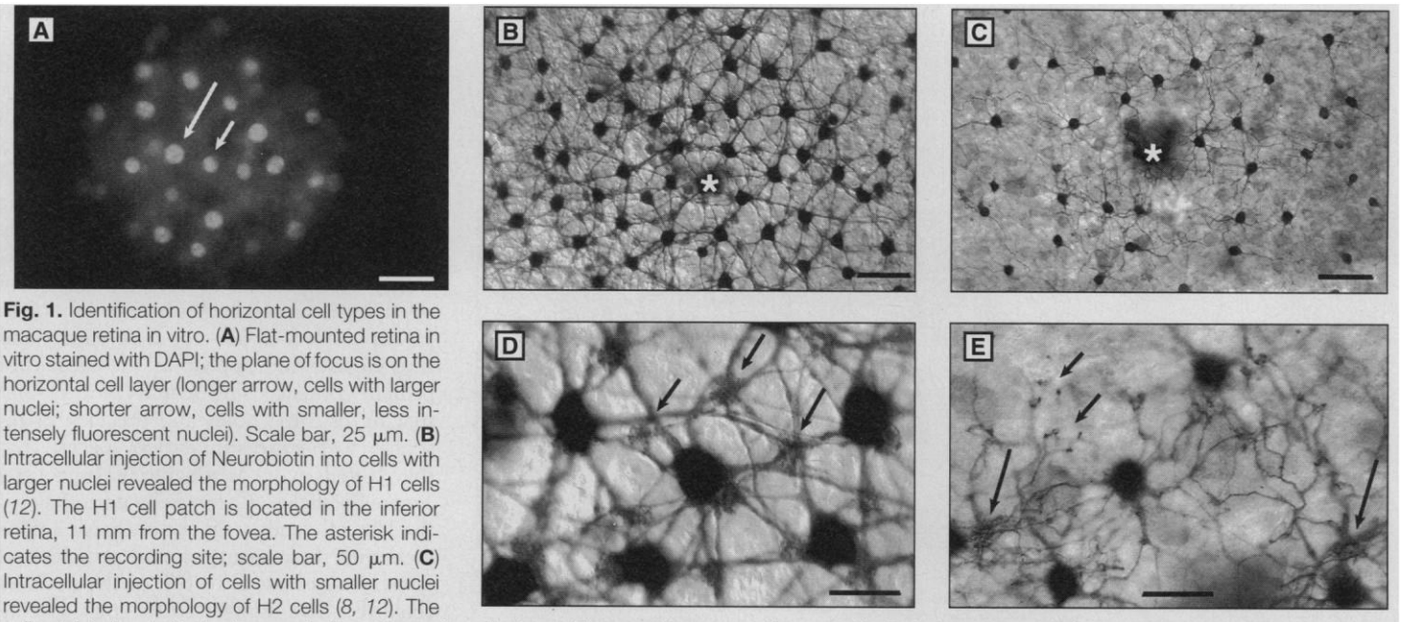

Fig. 1. Identification of horizontal cell types in the macaque retina in vitro. (**A**) Flat-mounted retina in vitro stained with DAPI; the plane of focus is on the horizontal cell layer (longer arrow, cells with larger nuclei; shorter arrow, cells with smaller, less intensely fluorescent nuclei). Scale bar, 25 μm. (**B**) Intracellular injection of Neurobiotin into cells with larger nuclei revealed the morphology of H1 cells (*12*). The H1 cell patch is located in the inferior retina, 11 mm from the fovea. The asterisk indicates the recording site; scale bar, 50 μm. (**C**) Intracellular injection of cells with smaller nuclei revealed the morphology of H2 cells (*8, 12*). The cell patch is located in the temporal retina, 10 mm from the fovea. The asterisk indicates the recording site; scale bar, 50 μm. (**D**) H1 cell dendritic network at higher magnification. The plane of focus is on the dendritic terminals that innervate and demarcate most of the cone pedicles (three pedicles are indicated by arrows). Scale bar, 15 μm. (**E**) H2 cell dendritic network at higher magnification. The plane of focus is on the dendritic terminals; most cone pedicles are sparsely innervated (short arrows), but a small subset of pedicles are densely innervated (longer arrows). Scale bar, 15 μm.

recordings from H1 cells also suggested an excitatory input from all three cone types (*4*). In contrast, others have reported that primate horizontal cells do make preferential cone connections, that a third horizontal cell type exists, and that spectral opponency should, therefore, originate at the level of the cone photoreceptor (*9*). Here, we used intracellular methods in an in vitro preparation of macaque retina to identify the functional and anatomical pathways between cones and horizontal cells.

In the in vitro retina, individual horizontal cell nuclei were fluorescently labeled and visually targeted under microscopic control for intracellular recording and staining (*10, 11*). Two cell populations were observed in the horizontal cell layer: a brightly labeled, regular mosaic of large nuclei, and a more dimly stained, less regular distribution of smaller nuclei (Fig. 1A). Intracellular staining with the tracer Neurobiotin (Vector, Burlingame, California) showed that the large and small cells corresponded to primate H1 and H2 cell types (*12, 13*). For both H1 and H2 cells, Neurobiotin passed into neighboring cells of the same type—presumably through gap junctions (*14*)—and revealed a "patch" of the cellular mosaic (Fig. 1, B and C). H1 cells had relatively large cell bodies, thick, radiating dendrites, and distinct, flowerlike clusters of dendritic terminals that contacted and clearly demarcated individual cone pedicles (Fig. 1, B and D). H2 cells had smaller cell bodies and thin, meandering dendrites that made only sparse contact with most of the cone pedicles (Fig. 1, C and E). The two cell types were also distinguished by the characteristic morphology of their axonlike processes (*12, 13*).

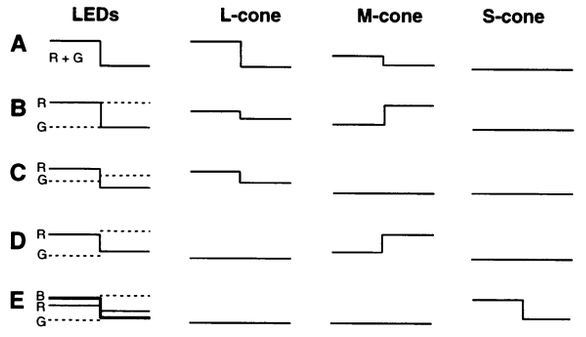

Fig. 2. Relative excitations of L-, M-, and S-cones in response to LED stimulus conditions. Red (R), green (G), and blue (B) LEDs have dominant wavelengths of 638, 554, and 445 nm, respectively. (**A**) Luminance modulation. The red and green LEDs are set to equiluminance and run in phase (blue LED off). This stimulus is most effective for the L- and M-cones; S-cone stimulation is negligible. (**B**) Chromatic modulation. The red and green LEDs are set to equiluminance and run in counterphase (blue LED off). During counterphase modulation, M-cones are more deeply modulated (M-cone contrast, 69%; L-cone contrast, 20%). (**C**) Selective L-cone modulation (L-cone contrast, 53%). (**D**) Selective M-cone modulation (M-cone contrast, 74%). (**E**) Selective S-cone modulation. The blue and red LEDs were modulated in counterphase with the green LED; modulation of the green LED was at 100% and the blue and red LEDs were reduced to 75% and 25% of maximum, respectively, to silence L- and M-cones (*27*) (S-cone contrast, 85%).

We recorded the light response of H1 and H2 cells by means of a trichromatic stimulator that was designed to identify cone photoreceptor activity. Light from three light-emitting diodes (LEDs) was delivered through the camera port of the microscope to the vitreal surface of the retina as a spot, 1° or 5° in diameter and modulated in time as square waves. The phase and radiance of the LED output were adjusted to give luminance flicker (Fig. 2A) or equiluminant chromatic flicker (Fig. 2B) (*15, 16*). The relative modulation amplitudes of the LEDs were adjusted by the method of silent substitution (*17*) to produce stimuli that would selectively modulate the L-, M-, or S-cones (Fig. 2, C through E) (*18*).

The LED stimulus revealed a clear difference in the physiological cone connections for the H1 and H2 cells. All H1 cells (n = 121) hyperpolarized to luminance increment (Fig. 3A), and they gave either no response or a very small amplitude modulation at twice the stimulus frequency to chromatic modulation (Fig. 3B). All H1 cells received a sign-conserving input from both L- and M-cones (Fig. 3, C and D). However, none of the H1 cells responded to selective stimulation of the S-cones (Fig. 3E). Thus, the H1 cell is not red-green opponent and appears to completely lack an input from S-cones.

Similarly, H2 cells (n = 36) also hyperpolarized to luminance modulation (Fig. 4, A and B), received a combined excitatory input from both L- and M-cones, and were not red-green opponent (Fig. 4, C and D). However, all H2 cells were also strongly hyperpolarized by selective stimulation of S-cones (Fig. 4E). The response of the H2 cell to the S-cone stimulus was of the same sign as and similar in amplitude to the response to either the L- or M-cone stimulus. Thus, the S-cone input to the H2 cell does not underlie a blue-yellow opponent signal.

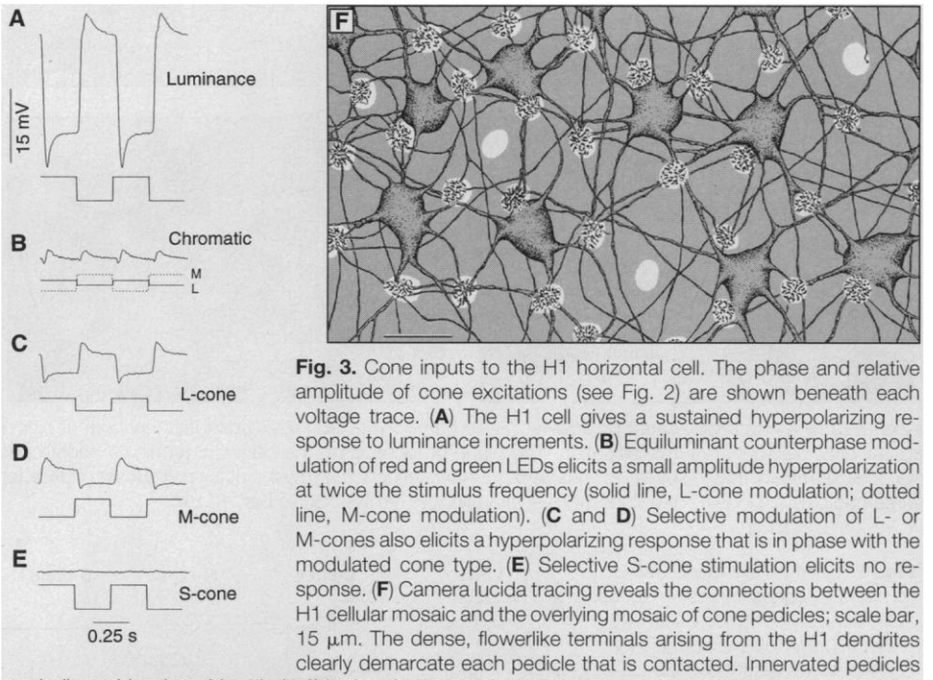

Fig. 3. Cone inputs to the H1 horizontal cell. The phase and relative amplitude of cone excitations (see Fig. 2) are shown beneath each voltage trace. (**A**) The H1 cell gives a sustained hyperpolarizing response to luminance increments. (**B**) Equiluminant counterphase modulation of red and green LEDs elicits a small amplitude hyperpolarization at twice the stimulus frequency (solid line, L-cone modulation; dotted line, M-cone modulation). (**C** and **D**) Selective modulation of L- or M-cones also elicits a hyperpolarizing response that is in phase with the modulated cone type. (**E**) Selective S-cone stimulation elicits no response. (**F**) Camera lucida tracing reveals the connections between the H1 cellular mosaic and the overlying mosaic of cone pedicles; scale bar, 15 μm. The dense, flowerlike terminals arising from the H1 dendrites clearly demarcate each pedicle that is contacted. Innervated pedicles are indicated by the white "holes" in the shaded background. The H1 cells contact almost all of the overlying cone pedicles (presumed L- and M-cones), but three cones in this field are skipped (7 to 8%; presumed S-cones), which accounts for the lack of S-cone input observed physiologically. Approximate positions of the "skipped" pedicles are indicated by the three "empty" holes in the mosaic.

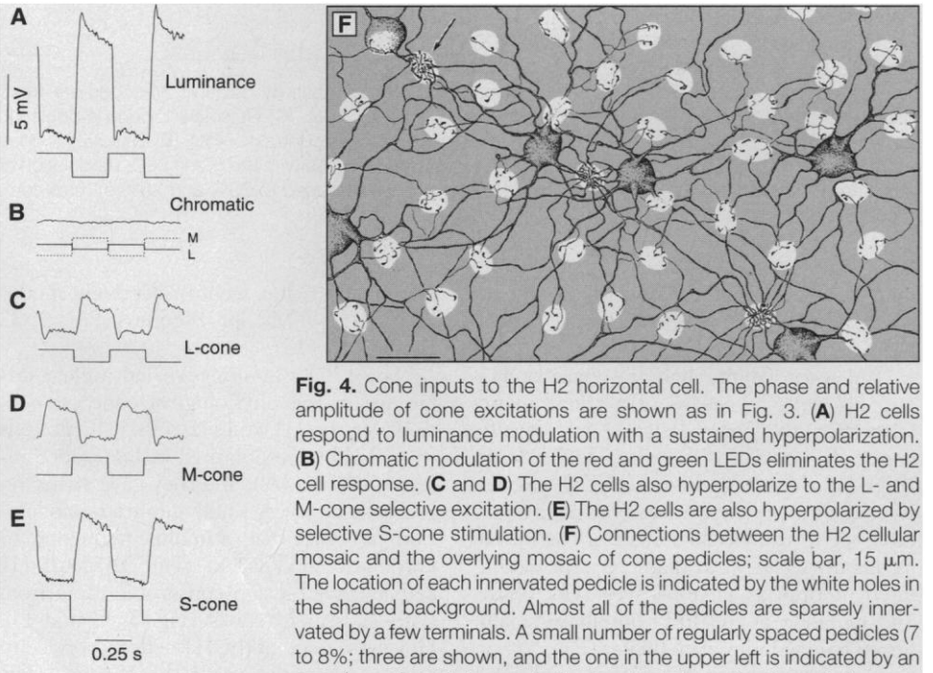

Fig. 4. Cone inputs to the H2 horizontal cell. The phase and relative amplitude of cone excitations are shown as in Fig. 3. (**A**) H2 cells respond to luminance modulation with a sustained hyperpolarization. (**B**) Chromatic modulation of the red and green LEDs eliminates the H2 cell response. (**C** and **D**) The H2 cells also hyperpolarize to the L- and M-cone selective excitation. (**E**) The H2 cells are also hyperpolarized by selective S-cone stimulation. (**F**) Connections between the H2 cellular mosaic and the overlying mosaic of cone pedicles; scale bar, 15 μm. The location of each innervated pedicle is indicated by the white holes in the shaded background. Almost all of the pedicles are sparsely innervated by a few terminals. A small number of regularly spaced pedicles (7 to 8%; three are shown, and the one in the upper left is indicated by an arrow) are densely innervated by terminals that arise through the convergence of dendrites from a number of surrounding H2 cells. These are presumed S-cones (*19*), and their selective contact with the H2 cell mosaic can account for its strong physiological response to selective S-cone stimulation.

The morphology of the H1 and H2 cell patches reveals the pattern of contact between cone pedicles and the horizontal cell dendritic networks (Figs. 1D, 1E, 3F, and 4F), which provides an anatomical basis for their different responses to cone-isolating stimuli. The H1 dendritic terminals (Fig. 3F) densely innervate the majority of overlying cone pedicles. However, counts of overlying cone cell bodies revealed that 7 to 8% of the cones are not innervated, and thus holes often appear in the mosaic of pedicle contacts. The scarcity and regular spacing of these holes and the lack of response to S-cone stimulation suggest that the H1 cells avoid or only rarely contact the S-cone pedicles. Conversely, terminals of the H2 cell dendrites make only sparse contacts with the majority of cone pedicles and densely innervate 7 to 8% of the pedicles (Fig. 4F). The number and regular spacing of these densely contacted pedicles, taken together with the H2 cells' response to S-cone stimulation, strongly suggest that these pedicles belong to S-cones (*19*).

We conclude that in trichromatic primates, including humans, spectral opponency does not arise from negative feedback from horizontal cells to cones. What, then, is the neural locus for a cone opponent transformation? Recent analysis of a blue-yellow opponent ganglion cell suggests, surprisingly, that antagonism between S-cone and L- and M-cone signals may arise from direct input to a bistratified ganglion cell dendritic tree from an ON-center bipolar cell that connects exclusively to S-cones and an OFF-center bipolar cell that connects to L- and M-cones (*10*). The circuitry that underlies red-green opponency and antagonism between L- and M-cones remains controversial (*20*).

If spectral opponency is not the role of the two horizontal cell types, what is their purpose in retinal function? Horizontal cells can contribute, through lateral connections, to the inhibitory receptive field surrounds of bipolar and ganglion cells (*21*). It has been suggested that both horizontal cell types connect similarly to all cones and function synergistically to form the surrounds of all ganglion cells (*22*). The primate H1 and H2 cell circuitries offer an alternative hypothesis: The two horizontal cell types contribute to the formation of parallel cone signal pathways at the first synaptic step in vision. Thus, H1 cells could contribute to pathways that transmit L- and M-cone signals only, whereas the H2 cells are concerned with the S-cone signal pathway. Because two horizontal cell types are present in most mammals, our primate results may reflect a general mammalian pattern.

REFERENCES AND NOTES

1. J. L. Schnapf, T. W. Kraft, D. A. Baylor, *Nature* **325**, 439 (1987).
2. C. A. Curcio, K. A. Allen, K. R. Sloan, C. L. Lerea, J. B. Hurley, *J. Comp. Neurol.* **312**, 610 (1991).
3. R. L. De Valois, C. J. Smith, S. T. Kitai, A. J. Karoly, *Science* **127**, 238 (1958); R. L. De Valois, G. H. Jacobs, I. Abramov, *ibid.* **146**, 1184 (1964); T. N. Wiesel and D. H. Hubel, *J. Neurophysiol.* **29**, 1115 (1966); P. Gouras, *J. Physiol. (London)* **199**, 533 (1968).
4. R. F. Dacheux and E. Raviola, *Proc. R. Soc. London* **239**, 213 (1990).
5. D. M. Schneeweis and J. L. Schnapf, *Science* **268**, 1053 (1995).
6. M. Kamermans and H. Spekreijse, *Prog. Retinal Eye Res.* **14**, 313 (1995).
7. D. A. Burkhardt, *Visual Neurosci.* **10**, 981 (1993).
8. H. Wässle, B. B. Boycott, J. Röhrenbeck, *Eur. J. Neurosci.* **1**, 421 (1989).
9. P. Ahnelt and H. Kolb, *J. Comp. Neurol.* **343**, 406 (1994).
10. D. M. Dacey and B. B. Lee, *Nature* **367**, 731 (1994).
11. Eyes from macaque (*Macaca nemestrina*, *Macaca fascicularis*, or *Macaca mulatta*) were enucleated after euthanasia. The retina, together with the pigment epithelium and choroid layer, was dissected and mounted in a superfusion chamber on the stage of a light microscope. Temperature was maintained in the chamber at 36° ± 1°C and superfused at ~5 ml/min. Vital labeling of horizontal cell nuclei was achieved by incubating the eye cup before retinal dissection for ~20 min in Ames medium to which diamidinophenylindole (DAPI) was added at a concentration of ~10 μM. Intracellular penetrations were made under direct visual control with high-resistance micropipettes, and light responses were recorded in conventional bridge mode. The recorded cells were directly observed during recording by iontophoretic injection of the fluorescent dye pyranine. At the termination of recording, cells were preserved for later analysis by injection of Neurobiotin and subsequent horseradish peroxidase histochemistry after tissue fixation (*10*).
12. H. Kolb, A. Mariani, A. Gallego, *J. Comp. Neurol.* **189**, 31 (1980).
13. B. B. Boycott, J. M. Hopkins, H. G. Sperling, *Proc. R. Soc. London* **229**, 345 (1987).
14. D. I. Vaney, *Prog. Retinal Eye Res.* **13**, 301 (1994).
15. V. C. Smith, B. B. Lee, J. Pokorny, P. R. Martin, A. Valberg, *J. Physiol. (London)* **458**, 191 (1992).
16. Output of the LEDs was modulated by a circuit driver under computer control (*23*). A spectroradiometric calibration was performed in the plane of the retina with a Gamma Scientific spectral radiometer. Radiometric measures were converted to photometric units (illuminance) by convolution with the human photopic spectral luminosity function (*24*). We estimated retinal illuminance in these experiments to be ~1000 trolands.
17. V. C. Smith, J. Pokorny, M. Davis, T. Yeh, *J. Opt. Soc. Am.* **12**, 241 (1995).
18. The relative LED modulations required for L-, M-, or S-cone isolation were calculated from the Smith-Pokorny cone fundamentals (*25*). Cone contrast was expressed as Michelson contrast $C = (Q_{max} - Q_{min})/(Q_{max} + Q_{min})$, where Q_{max} and Q_{min} correspond to the quantal absorptions calculated from the cone fundamentals. We confirmed S-cone isolation by checking for a null response in M-parasol ganglion cells, which were previously shown to lack S-cone input (*26*).
19. No other horizontal cell response properties or distinctive dendritic morphologies were found, despite our large sample of recorded cells. All of the morphological features attributed to a third (H3) horizontal cell type (*9*) were encompassed in our sample of H1 cells; H3 cells appear to reflect normal variation in the H1 cell population, with no separate physiological role. Our picture of the H1 and H2 cell mosaic is consistent with previous evidence that single cells can either avoid or "seek out" S-cones (*9*). This conclusion was recently confirmed by combining intracellular labeling of the horizontal cells and staining of the S-cone pedicles with an antibody to S-cone opsin [A. C. Goodchild, T. L. Chan, U. Grunert, *Soc. Neurosci. Abstr.* **21**, 1645 (1995)].
20. R. C. Reid and R. M. Shapley, *Nature* **356**, 716 (1992); P. Lennie, P. W. Haake, D. R. Williams, in *Computational Models of Visual Processing*, M. S. Landy and J. A. Movshon, Eds. (MIT Press, Cambridge, MA, 1991), pp. 71–82.
21. S. C. Mangel, *J. Physiol. (London)* **442**, 211 (1991).
22. R. G. Smith, *Visual Neurosci.* **12**, 545 (1995).
23. W. H. Swanson, T. Ueno, V. C. Smith, J. Pokorny, *J. Opt. Soc. Am.* **4**, 1992 (1987).
24. G. Wyszecki and W. S. Stiles, *Color Science: Concepts and Methods, Quantitative Data and Formulae* (Wiley, New York, 1982).
25. V. C. Smith and J. Pokorny, *Vision Res.* **15**, 161 (1975).
26. A. Valberg, B. B. Lee, P. K. Kaiser, J. Kremers, *J. Physiol. (London)* **458**, 579 (1992).
27. B. B. Lee and T. Yeh, in *Color Vision Deficiencies XII*, B. Drum, Ed. (Kluwer Academic, Dordrecht, Netherlands, 1995), pp. 177–184.

28. We thank the Regional Primate Center at the University of Washington for primate tissue; S. Buck, K. Boro, and P. Boro for their contributions; and B. Boycott, H. Wässle, H. Sherk, K. Mulligan, and M. Crognale for comments.

22 August 1995; accepted 11 December 1995

Molecular Detection of Primary Bladder Cancer by Microsatellite Analysis

Li Mao, Mark P. Schoenberg, Marshall Scicchitano, Yener S. Erozan, Adrian Merlo, Donna Schwab, David Sidransky*

Microsatellite DNA markers have been widely used as a tool for the detection of loss of heterozygosity and genomic instability in primary tumors. In a blinded study, urine samples from 25 patients with suspicious bladder lesions that had been identified cystoscopically were analyzed by this molecular method and by conventional cytology. Microsatellite changes matching those in the tumor were detected in the urine sediment of 19 of the 20 patients (95 percent) who were diagnosed with bladder cancer, whereas urine cytology detected cancer cells in 9 of 18 (50 percent) of the samples. These results suggest that microsatellite analysis, which in principle can be performed at about one-third the cost of cytology, may be a useful addition to current screening methods for detecting bladder cancer.

There are approximately 50,000 new cases of bladder cancer each year in the United States; it is the fourth most common cancer in men and the eighth most common in women (*1*). Urine cytology is a common noninvasive procedure for the diagnosis of this disease (*2*), but it can miss up to 50% of tumors (*3*). The "gold standard" for diagnosis is cystoscopy, which allows visualization and direct biopsy of suspicious bladder lesions. However, because cystoscopy is an expensive and invasive procedure, it cannot be used as a general screening tool for the detection of bladder cancer. Because early diagnosis of bladder cancer is critical for successful treatment, there is a pressing need for more sensitive and cost-effective diagnostic tools (*4*).

Multiple genetic changes occur during the development of primary bladder cancer (*5*). For example, mutations in the tumor suppressor gene p53 signal the progression to invasiveness and have been successfully used as molecular markers for the detection of cancer cells in urine samples (*6*). However, this diagnostic strategy has limited clinical application because the techniques are cumbersome and because p53 mutations appear relatively late in the disease (*6*, *7*).

We have suggested that microsatellite markers might be useful as clonal markers for the detection of human cancer (*8*) because simple DNA repeat alterations can be readily detected in clinical samples by the polymerase chain reaction (PCR). Here, we tested this suggestion in a pilot study of bladder cancer patients. We first screened 60 trinucleotide and tetranucleotide markers in the DNA from 50 anonymous primary bladder cancers (*9*). Of these cancers, 40 (80%) contained at least one marker alteration when compared with the DNA from matched normal lymphocytes. We calculated that a panel of the 10 most useful markers would theoretically detect alterations in 52% of all cancers (*10*).

Twenty-five patients presented with symptoms suggestive of bladder cancer (for example, gross hematuria) and were found to harbor suspicious lesions at cystoscopy. Urine samples were collected (before cys-

L. Mao, M. Scicchitano, A. Merlo, D. Schwab, D. Sidransky, Department of Otolaryngology—Head and Neck Surgery, Division of Head and Neck Cancer Research, Johns Hopkins University School of Medicine, 818 Ross Research, 720 Rutland Avenue, Baltimore, MD 21205–2196, USA.
M. P. Schoenberg, Department of Urology, Johns Hopkins Hospital, 600 North Wolfe Street, Baltimore, MD 21287, USA.
Y. S. Erozan, Department of Pathology, Johns Hopkins Hospital, 600 North Wolfe Street, Baltimore, MD 21287, USA.

*To whom correspondence should be addressed.